STABILITY OF GAS-FLUIDIZED BEDS

Kevin M. MANDICH[*] and Robert J. CATTOLICA

Department of Mechanical and Aerospace Engineering, University of California,
San Diego, La Jolla, CA, 92093, USA
*Corresponding author, E-mail address: kmandich@ucsd.edu

ABSTRACT

A temporal linear stability analysis is performed on the equations of motion which describe a bounded, vertical-pipe fluidized bed. This work provides a simple estimate of transition to bubbling for a given set of bed parameters.

It is found that the dependence of the level of instability on the particle diameter and density qualitatively matches the experimental observations of Geldart (1973) over a considerable portion of these particle parameters. Sharp increases in the growth constant at moderate fluidization velocities also reflect the bubbling phenomenon in fluidized beds. The growth constant rises when more particle-wall slip is allowed, and increases asymptotically with bed diameter.

Time signals of non-invasive pressure measurements of a lab-scale experiment are analysed in Fourier space, and the dominant frequencies compared to those obtained numerically. Qualitative agreement between the computational and experimental results was found to provide good evidence for the validity of the stability analysis.

NOMENCLATURE

d_p Mean particle diameter
D Bed diameter
e_w Particle-wall restitution coefficient
f Dominant frequency from experiment
F $= U_\infty^2/(gd_p)$ (Froude Number)
$F_{b,i}$ Interphase interaction force
g_i Body force
k Longitudinal disturbance wavenumber
L $= D/d_p$ (Dimensionless bed width)
n Azimuthal disturbance wavenumber
P_α Pressure
R $= \rho_f/\rho_s$ (Phase density ratio)
Re $= \rho_f d_p U_\infty/\mu_f$ (Reynolds number)
T Granular temperature
u_{mf} Minimum fluidization velocity
u_i Fluid-phase velocity
U_∞ Far-wall fluid velocity
u_t Terminal velocity of a particle in free-fall
v_i Solid-phase velocity

α Subscript value; $\alpha = f$ or s for fluid or solid phase
δ_o Continuum-averaging length scale
ϕ Solid-phase volume concentration
ϕ' Specularity coefficient
Γ Granular temperature generation
λ Granular conductivity
μ_α Shear viscosity
η_α Bulk viscosity
ξ Particle sphericity
ρ_α Density
σ Complex disturbance frequency
σ^α_{ij} Stress tensor

Hats represent perturbed functions of r, "o" subscripts represent base-state functions, and primes denote differentiation with respect to r.

INTRODUCTION

It is often desirable to consider the effects of particle-phase mixing when designing fluidized bed applications. Some processes would find it advantageous to maximize the level of particle mixing while minimizing the energy spent forcing the fluid through the medium. Another investigator may wish to maximize the interstitial fluid velocity, and thus the heat and mass transfer characteristics of the bed, without experiencing the oftentimes undesirable pressure fluctuations inherent with higher fluidization velocities. In both cases the important factor is the stability of the bed, manifested through voidage fluctuations.

Disturbances in space and time are either dampened or they are dramatically and rapidly amplified into regions of large voidage, also known as bubbles (Kunii & Levenspiel, 1991). Geldart (1973) created an empirical road map for fluidized bed behavior as a function of particle diameter and density based upon his experimental observations. The current work develops a model to predict the stability characteristics of a fluidized bed for the full range of parameters – fluidization velocity, voidage, disturbance length and time scales, fluid-phase density and viscosity, and the effect of boundaries – in addition to the particle diameter and density. Although only a fluid phase with negligible inertial and viscous effects is considered, it is straightforward to extend the current work to liquid-fluidized beds.

The stability of fluidized beds has been featured in numerous works. Anderson & Jackson (1968) and Batchelor (1988) considered the effects of solid-phase pressure on the stability of fluidized beds. Koch and Sangani (1999) employed a numerical simulation to determine the particle velocity variance, and applied the results to a linear stability analysis of a fluidized bed. Didwania (2001) also included granular temperature considerations in his analysis of an unbounded fluidized bed. The present analysis uses similar tactics as the last work but for a flow bounded by a rigid tube.

A linear analysis greatly simplifies the problem. Full CFD simulations of gas-particle flows solve the complete nonlinear equations of motion over time and space, but usually at exorbitant computational costs. The present work attempts to create an estimate for instabilities leading to the onset of bubbles using a relatively inexpensive method. Doing so allows one to obtain critical stability information for a wide range of parameters in liquid- and gas-fluidized beds in a matter of minutes on a personal computer. The results of this technique are compared to previously-observed experimental patterns of bubbling and instability. Fluid pressure time signals taken from lab-scale experiments are also analysed in Fourier space, and the dominant frequencies are compared to those obtained through the computation.

MODEL DESCRIPTION

The flow under consideration is shown in Figure 1. Base-state profiles of the fluid-phase velocity and the granular temperature are represented, not to scale.
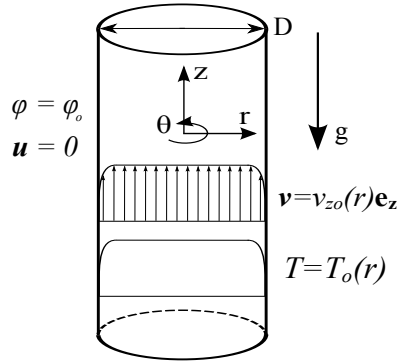
Figure 1: Base-state flow configuration

Governing Equations

The two phases are assumed to be interpenetrating continua. The continuum-averaged equations of motion have been derived and introduced elsewhere (Koch & Sangani, 1999; Didwania, 2001) and are listed here.
Continuity:

$$\frac{\partial \phi}{\partial t} + \nabla \cdot (\phi \vec{u}) = 0 \quad (1)$$

$$\frac{\partial (1-\phi)}{\partial t} + \nabla \cdot (1-\phi)\vec{v} = 0 \quad (2)$$

Momentum:

$$\rho_s \phi \left(\frac{\partial \vec{u}}{\partial t} + \vec{u} \cdot \nabla \vec{u} \right) = \nabla \cdot \underline{\underline{\sigma}}^s + \phi \nabla \cdot \underline{\underline{\sigma}}^f + \vec{F}_b + \phi \rho_s \vec{g} \quad (3)$$

$$\rho_f (1-\phi) \left(\frac{\partial \vec{v}}{\partial \hat{t}} + \vec{v} \cdot \nabla \vec{v} \right) = (1-\phi) \nabla \cdot \underline{\underline{\sigma}}^f - \vec{F}_b + (1-\phi) \rho_f \vec{g} \quad (4)$$

Solid-phase granular temperature:

$$\frac{3}{2} \rho_s \phi \left(\frac{\partial T}{\partial t} + \vec{u} \cdot \nabla T \right) = \underline{\underline{\sigma}}^s : \nabla \vec{u} + \nabla \cdot (\lambda \nabla T) + \Gamma \quad (5)$$

The last equation is represents a balance of the pseudo-thermal energy of the particle phase, otherwise known as the granular temperature. This quantity is a measure of the particle velocity variance whose inclusion is gas-particle flows is now standard for closing the equations of motion; see Goldhirsch (2003) for a review. Both phases are assumed to be Newtonian. The solid-phase stress is:

$$\underline{\underline{\sigma}}^s = -P_s(\phi, T)\underline{\underline{I}} + 2\mu_s(\phi, T)\underline{\underline{D}}^s + \eta_s(\phi, T)\nabla \cdot \vec{u} \quad (6)$$

With deviatoric stress tensor:

$$\underline{\underline{D}}^s = 0.5(\nabla \vec{u} + \nabla \vec{u}^T) \quad (7)$$

Similar expressions hold for the fluid phase. These equations are non-dimensionalized using length D, velocity U_∞, time D/U_∞, ρ_s, d_p, and dimensionless parameters L, F, R and Re. In the case of gas-fluidized beds, terms proportional to R may be neglected. The axisymmetric, steady, base-state solution for the fluid-phase velocity $v_{zo}(r)$ is acquired analytically via integration of (4), while the granular temperature profile $T_o(r)$ is obtained by solving the nonlinear equation (5) numerically. The boundary conditions for each variable are the base-state versions of (12), (15), and (16). The expression for the interphase drag force term F_b is the same as that used by Anderson and Jackson (1968):

$$\vec{F}_b = (1-\phi)(\vec{v} - \vec{u}) \frac{(\rho_s - \rho_f)g}{u_t} \phi(1-\phi)^{1-N} \quad (8)$$

Here, N is the Richardson-Zaki (1954) exponent, taken as a constant value of 3 considering the small range of Re considered in this work. Closure expressions for μ_s, η_s, λ, P_s, and Γ are derived from the kinetic theory of granular flows and critical-state soil mechanics. The particular set used comes from the work of Didwania (2001), which bridges the gap between the regimes of purely collisional interaction and fully frictional flow.

Linear Stability Analysis

The variables are perturbed about their base-state solutions:

$$\psi(r, \theta, z, t) = \psi_o(r) + \tilde{\psi}(r, \theta, z, t) \quad (9)$$

Where ψ is the nine-term, dimensionless solution vector:

$$\psi = \begin{pmatrix} u_r & u_\theta & u_z & v_r & v_\theta & v_z & T & P & \phi \end{pmatrix}^T \quad (10)$$

The perturbed variables are assumed to be normal modes:

$$\tilde{\psi}(r, \theta, z, t) = \hat{\psi}(r) e^{i(kz + n\theta) + \sigma t} \quad (11)$$

Here, k represents the longitudinal wavenumber of the disturbance and $\sigma = \sigma_r + i\sigma_i$ is the complex frequency. The real part of σ is the growth constant and the imaginary part is the disturbance frequency. A positive growth constant represents a disturbance whose amplitude increases exponentially in time, whereas a negative value of σ_r decreases in time. The linearized equations of motion may be represented in matrix form:

$$\frac{\partial \hat{\psi}}{\partial t} = \underline{\underline{A}} \hat{\psi} \quad (12)$$

The boundary conditions along the centerline are dictated by the coordinate system:

$$\lim_{r \to 0} \frac{\partial}{\partial \theta} \begin{bmatrix} \hat{\mathbf{u}} & \hat{\mathbf{v}} & \hat{T} & \hat{P} & \hat{\phi} \end{bmatrix} = 0 \quad (13)$$

The condition for each variable is dependent upon the value of n. In the case of $|n|=1$, two pairs of conditions lose their linear independence, so each continuity equation is applied in the limit as $r \to 0$:

2

$$2\hat{u}'_r + i\hat{u}'_\theta = 0 \qquad\qquad 2\hat{v}'_r + i\hat{v}'_\theta = 0 \qquad (14)$$

At the wall, impermeability is enforced by setting the r-components of each velocity to zero. Conditions for the tangential solid-phase velocities and granular temperature are borrowed from Johnson & Jackson (1987):

$$\mathbf{n}\cdot\hat{\boldsymbol{\sigma}}^s\cdot\mathbf{t} = L\frac{\sqrt{3}\pi\phi_o\phi'}{6\phi_p\left(1-\left(\phi_o/\phi_p\right)^{1/3}\right)}T_o^{1/2}\hat{\mathbf{u}}\cdot\mathbf{t} \qquad (15)$$

$$\mathbf{n}\cdot\left(\lambda\nabla\hat{T}\right) = L\frac{3\sqrt{3}\pi\phi_o\left(1-e_w^2\right)}{8\phi_p\left(1-\left(\phi_o/\phi_p\right)^{1/3}\right)}T_o^{1/2}\hat{T} \qquad (16)$$

Here, ϕ' is the specularity coefficient and e_w is the particle-wall restitution coefficient. These parameters are measures of the particle-phase-to-wall frictional interaction and transfer of pseudo-thermal energy to the wall, respectively. Partial slip conditions for the fluid phase are adopted from the work of Sinclair & Jackson (1989):

$$\mathbf{n}\cdot\hat{\boldsymbol{\sigma}}^f\cdot\mathbf{t} = \frac{2}{\delta_o}\frac{\phi_p}{\phi_o}\left(T_o\hat{\mathbf{v}} + \mathbf{v}_o\hat{T}\right)\cdot\mathbf{t} \qquad (17)$$

Computational Methods

The base-state granular temperature field $T_o(r)$ was solved via an iterative relaxation method using Chebyshev spectral collocation for T_o. The solution was checked by direct integration of (5) from the wall to the constant far-wall value of T_o, given as the solution of $\Gamma=0$. The wall conditions of the matrix method were used as the initial conditions for the Runge-Kutta 4 (RK4) integration.

The linearized system (12)-(17) was solved using a staggered-grid Chebyshev spectral collocation scheme. The solutions for P and ϕ were resolved on staggered grid points, eliminating the need for artificial boundary conditions for these variables. The linearized equations were resolved at the $N+1$ Gauss-Lobatto points, while the solid-phase continuity and r-fluid-phase momentum equations were resolved on the maxima of the Chebyshev polynomial of degree N. A set of interpolating matrices interpolated between the staggered points and the grid points.

The number of grid points $N+1$ was increased until the leading eigenvalues were insensitive to grid resolution. The value of the $5N-4$ eigenvalues with the greatest real part, for one set of parameters, is the leading eigenvalue. The maximum leading eigenvalue over the spectrum of longitudinal wavenumbers k indicates the dominant mode.

The numerical method was first validated by reproducing the stability results of Hagen-Poiseuille flow for a single fluid (Khorrami et al., 1989). A second check consisted of discretizing the domain from wall to wall for the $n = 0$ case and applying an artificial boundary condition for the non-staggered variable ϕ. Finally, the linearized equations were integrated directly from $r = 1$ to $r = 0.1$ via an RK4 method with mesh refinement, and using the wall conditions from the Chebyshev method as the initial conditions. The latter two methods checked the accuracy of the resolved eigenvalue and eigenfunctions, respectively.

RESULTS

Computational Results

A typical stability diagram for the first several azimuthal modes are shown in Figure 2.
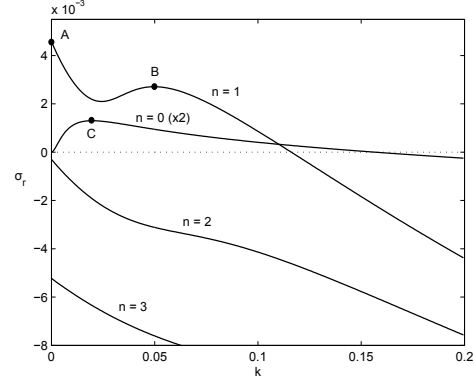
Figure 2: Growth constant vs. wavenumber k for various values of n.

Points A, B, and C represent the three possible dominant mode families at any value of the bed parameters. The B and C modes vary in z and θ, while the A mode varies only in the angular direction. All three are identified and considered because, although the A mode tends to be the least stable, it is possible that the others may become important in a secondary instability or nonlinear analysis. The order of the growth constants (A>B>C) is typical for most arrangements, although at certain extremes the B or C disturbance families may become dominant. An example of this is shown in Figure 3.
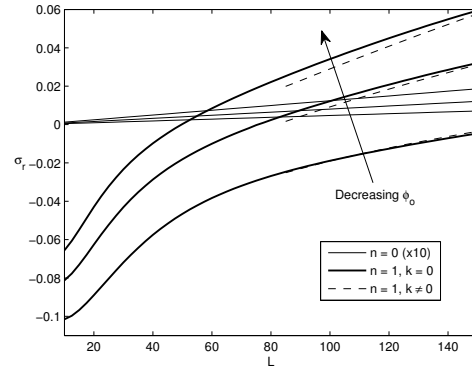
Figure 3: Growth constant versus dimensionless bed diameter for $\phi_0 = 0.49, 0.52, 0.55$.

All three mode families exhibit a monotonic increase with the dimensionless channel width. At low values of L, the axisymmetric mode C is dominant, although the A disturbance becomes so as L is increased. The point at which this transition occurs increases dramatically as the base-state voidage decreases. In addition, all modes are less stable for higher values of ϕ_o for every value of L considered. The B family of disturbances shows up only after a certain channel width. At lower values of L the stability curve for $n = 1$ resembles the $n = 2$ curve seen in Figure 2, and due to the ambiguity of defining a traveling disturbance with no peak in the curve, the B family is ignored.
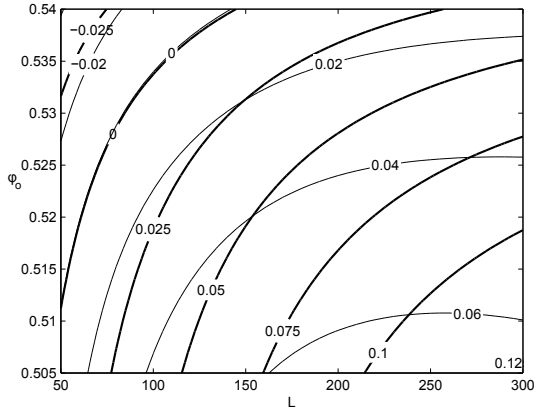
Figure 4: Maximum growth constant σ_r (bold lines) and corresponding frequency σ_i of the $n = 1$ modes as a function of ϕ_o and L.

Figure 4 displays a contour plot of the growth constant and frequency of the A disturbance family in the L-ϕ_o plane. The axisymmetric family is ignored for simplicity. The growth constant increases monotonically with L at all values of ϕ_o and asymptotically approaches a constant value. As the channel width increases to very large values, the effect of the boundaries fades and the bed begins to resemble an unbounded configuration. Also notable is how the rate of increase of the growth constant with respect to the channel width is lower at higher values of ϕ_o. This is a result of the higher solid-phase viscosity and pseudo-thermal conductivity of more packed beds, and suggests that the dissipation of energy due to particle interactions begins to trump the input of energy from the fluid phase.

The disturbance frequency of the stationary mode increases with the channel width at low to moderate values of L, followed by a decrease at higher values. This means that at every value of ϕ_o, there is a channel width which yields disturbances with the highest frequency. The value of the channel width at which the maximum occurs is lower for less-packed beds.
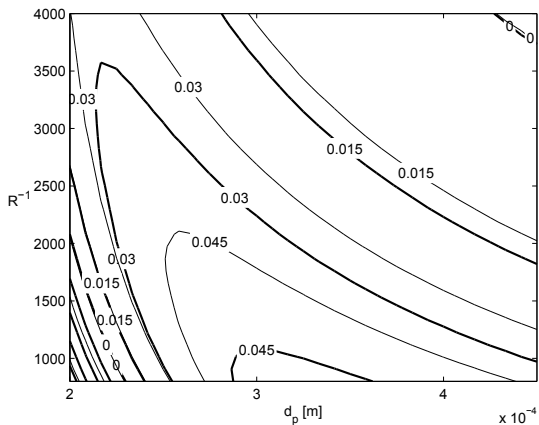
Figure 5: Maximum growth constant σ_r (bold lines) and corresponding frequency σ_i of the $n = 1$ modes as a function of R^{-1} and d_p.

Figure 5 shows a contour plot of the growth constant and corresponding frequency of the non-axisymmetric family in the d_p-R^{-1} plane. At each value of the phasic density ratio R^{-1}, which is proportional to the particle density, the growth constant and frequency increase with a larger

particle diameter up to a maximum value, and is followed by a decrease thereafter. This behavior is attributed to the balances between two pairs of terms in the formulation. The first is the classically-recognized balance between the dimensionless drag force fluctuation term β_ϕ and the body force term F_b (Didwania, 2001). The former term is responsible for destabilization of the flow and the latter plays a stabilizing role. The second balance lies between the stabilizing effect of the viscous, conductive, and dissipation terms, and the destabilizing effect of the granular temperature generation due to interparticle collisions.

When compared to the particle classification map of Geldart (1973), some patterns are shared between the two. The lower-left-hand side of Figure 5 corresponds to the edge of the Geldart A classification of particles, characterized by a considerable level of bed expansion before the appearance of bubbles. The upper-right corner of this plot corresponds to Geldart D particles, in which bubbling is uncommon at lower fluidization velocities and usually gives way to spouting at higher U_∞/u_{mf}. The majority of the contour plot corresponds to the Geldart B particle regime, with the regions of the highest growth constant corresponding to the greatest B-type behavior. Beds composed of this particle type generally exhibit bubbling right at $U_\infty/u_{mf} \approx 1$. There is a parallel between the bubbling that is experimentally observed and the computed level of instability as functions of particle diameter and density. Traces of the growth constants versus U_∞/u_{mf} for the three primary disturbance families are shown in Figure 6 for several values of the base-state solid-phase concentration.
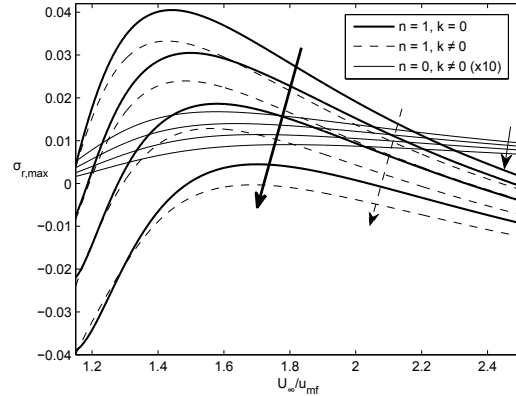
Figure 6: Growth constant of the A, B, and C disturbance families versus fluidization velocity for $\phi_0 = 0.505$, 0.515, 0.525, 0.535. Arrows indicate direction of increasing ϕ_0.

All three mode families exhibit a dramatic increase in the growth constant with fluidization velocity up to a value of $U_\infty/u_{mf} = 1.4$-1.6. After a certain point, however, the growth constants decrease monotonically with higher fluidization velocities. This behavior, opposite to that seen in experiment, appears to be a breakdown of the linear assumption at higher velocities. However, the point of the current analysis is to identify the linear disturbances which, when amplified, evolve into bubbles through a cascade of secondary and nonlinear interactions. The level of fluidization at $U_\infty/u_{mf} = 1.4$ is generally well within the bubbling regime for all Geldart particles. With this in mind, the present analysis yields a qualitative similarity to the dependence of stability and bubbling within the fluidization regime immediately after $U_\infty=u_{mf}$.
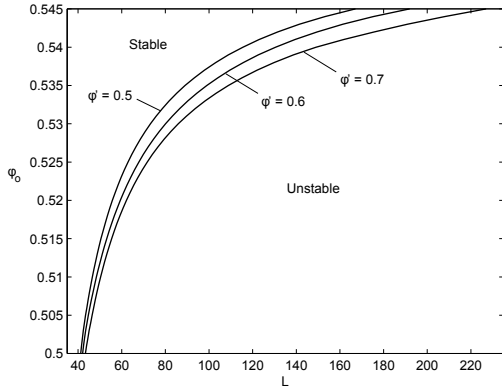
Figure 7: Neutral stability contours ($\sigma_{r,max} = 0$) of the non-axisymmetric disturbance at varying levels of particle-wall slip.

Figure 7 presents marginal stability curves for the $n = 1$ mode in the L-ϕ_o plane for three values of the specularity coefficient of (15). Systems which allow for more tangential particle slip at the wall have a higher area of instability in the L-ϕ_o plane. The lesser amount of "clamping" of the u_θ and u_z eigenfunctions lowers shear rates throughout the domain, thereby reducing viscous dampening. The difference in channel width values at a fixed value of ϕ_o for the marginal stability traces grows as the bed becomes more closely-packed. This indicates that the effect of the boundary conditions is felt more throughout the domain as the base-state voidage decreases.

(a)

(b)
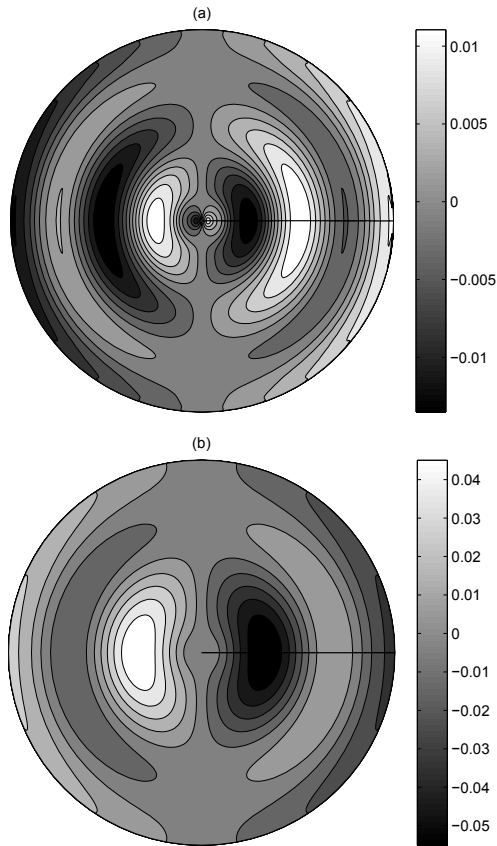
Figure 8: Eigenfunctions of the perturbed solid volume concentration ϕ for the (a) $n = 1, k = 0$ and (b) $n = 1, k \neq 0$ modes.

Figure 8 presents eigenfunction plots for the perturbed solid volume concentration for the non-axisymmetric

modes A and B of Figure 1. The A eigenfunction exhibits a larger amount of fluctuation in r than that of the B mode. The stability resulting from the large amount of viscous dissipation expected from this behavior is not realized when considering that the first mode does not vary in the z-direction. Interesting to note are the magnitudes of each function. The B mode exhibits a maximum amplitude over four times that of the A disturbance. Considering that the growth constants of these two modes are usually on the same order and comparable in magnitude to one another (see Figures 3 and 6), it seems probable that the $k \neq 0$ mode will remain important when nonlinear interactions become appreciable.

Experimental Results

A series of lab-scale experiments was performed on three bed materials. Each bed was fluidized using atmospheric air at varying levels of superficial gas velocity. Table 1 summarizes the relevant parameters for each particle. Figure 9 shows a schematic of the experimental set-up.

	ρ_s [kg m^{-3}]	d_p [µm]	ϕ_o	ξ
Material 1	1250	123	0.54	0.9
Material 2	2700	334	0.53	0.9
Material 3	3560	430	0.53	0.9

Table 1: Particle parameters used in experiment

The solid-phase volume fraction was determined by measuring the mass of and the volume filled by the bed at loose packing (not settled).
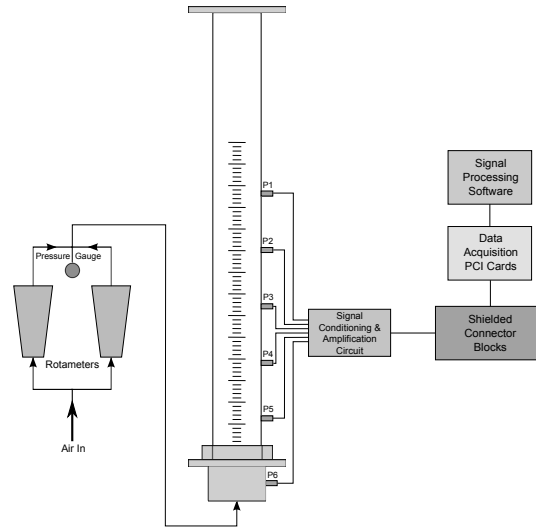
Figure 9: Experimental schematic. Pressure taps are denoted P1-P6.

The pressure signals were sampled at a rate of 200Hz. These time signals were analysed in Fourier space, and the frequency component with the highest amplitude was identified as dominant. Normalized dominant frequency values obtained from the P4 tap, averaged from three separate runs, are shown in Figure 10. Frequencies of the dominant mode obtained from the numerical analysis are displayed in Figure 11.
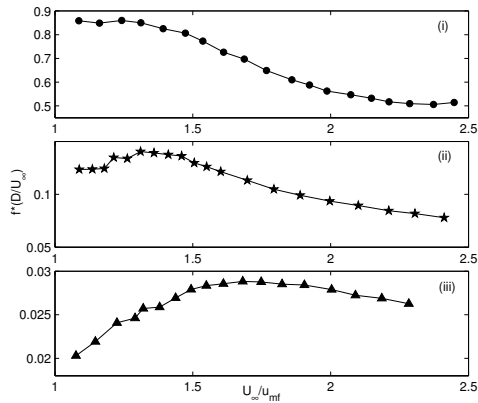
Figure 10: Normalized experimental frequencies of the dominant mode as a function of fluidization velocity. (i) Material 1; (ii) Material 2; (iii) Material 3.
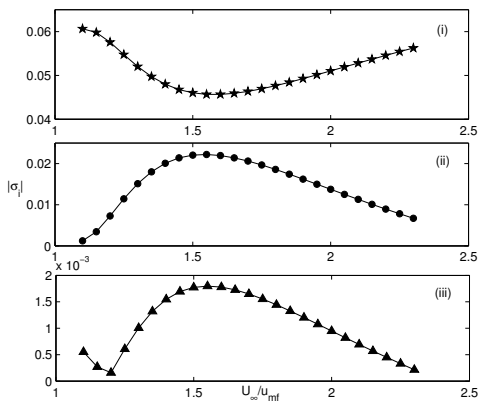
Figure 11: Numerically-obtained disturbance frequencies of the dominant mode as a function of fluidization velocity. (i) Material 1; (ii) Material 2; (iii) Material 3.

Most notable is the reduction in normalized frequency as the particle diameter and density increase. In addition, all three materials exhibit a decrease in disturbance frequency as the fluidization velocity is increased. For the latter two materials, an increase in the absolute disturbance frequency is present at the lower fluidization velocities. The absolute value is responsible for the inverted shape of Figure 11(i). The simulation predicts a negative disturbance frequency for this data set, corresponding to a disturbance with a phase velocity travelling against the mean flow.

CONCLUSION

A linear stability analysis provides a simple means of estimating the transition to bubbling in a fluidized bed over a large range of flow parameters. The dominant disturbance was found to be one of three separate modes determined by the particular set of parameters chosen. The analysis predicts a decrease in stability with increasing fluidization velocity for U_∞/u_{mf} ranging from 1.1 to 1.4, the range corresponding to smooth fluidization and the beginning of the bubbling regime. Mapping the growth constant as a function of particle diameter and density reveals a dependence upon these parameters similar to that of the empirical bubbling diagram of Geldart (1973). The growth constant is also found to increase asymptotically with the dimensionless channel width, and to decrease when more particle slip is allowed at the wall. With all other parameters being held constant, beds with a lower

base-state solid-phase concentration are found to be less stable than those with a higher ϕ_0, another similarity to fluidized bed behavior.

While the present analysis provides useful and intuitive results, the limitations must also be considered. The anisotropy resulting from the unidirectional energy input to the granular temperature is ignored. This becomes more appreciable at higher fluidization velocities as well as near the boundaries. The limitations of the theoretical model leave something to be desired, as well. The continuum assumption for the solid phase is reasonable only at large length scales. Therefore, one must be cautious concerning the validity of the results at small values of the dimensionless channel width. Also, as mentioned, the presence of bubbles disqualifies the small-amplitude assumption central to the linear problem. The primary goal of the present work was to identify the fundamental modes of instability which may either remain dominant or work in conjunction with the other linear and secondary modes as the fluidization velocity increases. At fluidization velocities immediately after u_{mf}, however, the linear analysis is a useful tool.

REFERENCES

ANDERSON, T.B. & JACKSON, R. (1968) "A Fluid Mechanical Description of Fluidized Beds – Stability of the State of Uniform Fluidization" *Indust. Engng. Chem. Fundam.* **7**, 12-21.

BATCHELOR, G.K. (1988) "A New Theory of the Instability of a Uniform Fluidized Bed" *J. Fluid. Mech.* **193**, 75-110.

DIDWANIA, A.K. (2001) "A New Instability Mode in Fluidized Beds" *Europhysics Letters*, **53 (4)**, 478-482.

GELDART, D. (1973) "Types of Gas Fluidization" *Powder Technology*, **7 (5)**, 285-292.

GOLDHIRSCH, I. (2003) "Rapid Granular Flows" *Ann. Rev. Fluid Mech.* **35**, 267-293.

JOHNSON, P.C. & JACKSON, R. (1987) "Frictional-collisional constitutive relations for granular materials, with application to plane shearing" *J. Fluid. Mech.* **176**, 67-93.

KHORRAMI, M.R., MALIK, M.R., & ASH, R.L. (1989) "Application of Spectral Collocation Techniques to the Stability of Swirling Flows" *J. Comp. Phys.* **81**, 206-229.

KOCH, D.L. & SANGANI, A.S. (1999) "Particle pressure and marginal stability limits for a homogeneous monodisperse gas-fluidized bed" *J. Fluid. Mech.* **400**, 229-263.

KUNII, D. & LEVENSPIEL, O. (1991) *Fluidization Engineering*, Second Edition, Butterworth-Heinemann.

RICHARDSON, J.F. & ZAKI, W.N. (1954) "Sedimentation and Fluidization: Part I." *Trans. Inst. Chem. Engrs.* **32**, 35-53.

SINCLAIR, J.L. & JACKSON, R. (1989) "Gas-Particle Flow in Vertical Pipes with Particle-Particle Interactions" *AIChE* **25 (9)**, 1473-1486.